THE BELL SYSTEM TECHNICAL JOURNAL
Vol. 56, No. 10, December 1977
Printed in U.S.A.

WT4 Millimeter Waveguide:

TE_{01} Transmission in Waveguide with Axial Curvature

By J. W. CARLIN and S. C. MOORTHY

(Manuscript received April 7, 1977)

In this paper we examine the relationship between the loss of the TE_{01} mode in a multimode circular waveguide and the waveguide geometry. First-order perturbation theory solutions of the coupled line equations were used to predict the loss from measurements of the waveguide geometry. The predicted loss disagreed with the measured loss for the 14 km long waveguide line in the WT4 field evaluation test. An analysis of the coupled line equations which considers the effects of both first- and second-order mode conversion is described. The appropriate coupling coefficients are derived and discussed. Second-order perturbation theory solutions of the coupled line equations are developed and examined. Losses predicted from the measured waveguide curvature and the second-order theory agree well with measured loss data. The results indicate that axial curvature leads to significant mode conversion-reconversion effects between the TE_{01}–TM_{11}, TE_{01}–TE_{12}, TM_{11}–TM_{21}, TE_{12}–TM_{21} modes in the installed waveguide of the WT4 field evaluation test. The TM_{21} conversion is due to curvature fluctuations with a characteristic wavelength of 10 to 30 m.

I. INTRODUCTION

The transmission characteristics of the TE_{01} mode in circular waveguide are quite different from the characteristics of cable or wire transmission media currently used in the Bell System. The waveguide medium has the unique property that its heat loss decreases with increasing frequency. Heat losses[1] as low as 0.3 dB/km are obtained at 110 GHz in 60 mm diameter waveguide. However, since the diameter of the

waveguide is much larger than the operating wavelength of 2.75 mm at 110 GHz, several hundred spurious modes can also propagate, in addition to the TE_{01} mode. The spurious modes have slightly different phase and group velocities than the TE_{01} mode. Spurious modes are excited in practice because the waveguide is not a geometrically perfect right circular cylinder, and there is a continuous exchange of energy between the TE_{01} and spurious modes. This mode conversion-reconversion results in added loss and delay distortion. A detailed understanding of the relationship between spurious mode generation and waveguide geometry is required since even small distortions in the guide cross section (of the order of 1 μm) can cause substantial loss.[2]

The mode conversion problem can be modeled by an infinite system of coupled transmission line equations[3] for which approximate solutions have been obtained by first-order perturbation theory.[4] At the beginning of the WT4 field evaluation test the first-order theory was considered to be a valid and accurate method for predicting the TE_{01} mode conversion loss. Detailed measurements of the waveguide cross-section geometry were carried out in the laboratory on 9 m long individual sections of waveguide. The curvature of the waveguide axis, in two orthogonal planes, was also measured over the 14 km field evaluation test route. The curvature and cross-section geometry data and the first-order perturbation theory solutions were used to predict the TE_{01} mode conversion loss. Waveguide curvature was found to be a significant source of TM_{11} and TE_{12} mode generation with a predicted TE_{01} mode conversion loss of approximately 0.2 dB/km at 110 GHz. All other predicted first-order mode conversion effects resulted in an additional TE_{01} loss of less than 0.03 dB/km at 110 GHz.

The measured loss disagreed substantially with those first-order predictions. The measured loss indicated a total TE_{01} mode conversion loss of approximately 0.5 dB/km at 110 GHz.

In this paper, we show that the generation of the TM_{21} mode is a significant source of TE_{01} mode conversion loss in curved waveguide. The TM_{21} mode is not coupled directly to the TE_{01} mode and therefore is ignored in the first-order perturbation theory. It is excited via the TM_{11} and TE_{12} modes and hence can be thought of as a "second-order" phemonenon. However, as we shall see, the energy coupled into the TM_{21} mode exceeds the energies coupled into the "first-order modes" TM_{11} and TE_{12} under certain conditions. Therefore the term "second order" is used to describe any theory which includes the TM_{21} mode, only in the sense that it is a mode which is indirectly excited from the TE_{01} mode.

An approximate model and a second-order perturbation theory is developed for the TM_{21} conversion in curved waveguide, which, in conjunction with the first-order theory for TM_{11} and TE_{12} conversion,

yields results which agree well with measured results. The source of the TM_{21} generation is identified as waveguide curvature with low spatial frequency components with a characteristic wavelength of 10 to 30 meters.

II. PROBLEM FORMULATION

Maxwell's equation in the deformed waveguide may be transformed to an infinite set[3,5] of coupled transmission line equations expressed in terms of the normal modes of the undeformed guide:

$$\frac{d}{dz} A_m(z) = \sum_{n \neq m} K_{m,n}(z) A_n(z) - j h_m A_m \tag{1}$$

The unknowns in eq. (1) are the normal mode amplitudes A_m while h_m are the normal mode propagation constants in the undeformed guide. The sum over n extends over an infinite number of modes, and the coefficients $K_{m,n}$ in the infinite system of equations consist of the product of a geometry deformation factor and a normalized coupling[4,5,6,7] coefficient $C_{m,n}$. The derivation of the coupled line equations and the normalized coupling coefficients, as well as some notation for normal modes, is outlined in the appendix.

We shall use single subscripts m and n when referring to a general normal mode. A double subscript pn is used in referring to a specific normal mode such as TE_{pn} or TM_{pn}. Here the p refers to the order of the azimuthal variation ($\cos p\phi$ and $\sin p\phi$) while the n is the order of the radial variation $J_p(x_n r)$. The modes in dielectric-lined waveguide, the principal transmission medium in the field evaluation test, are not strictly[6,7,8] "transverse electric" TE or "transverse magnetic" TM but we will retain the notation. The axis of the installed waveguide is a curve in three-dimensional space. The polarizations of the locally excited spurious modes are related to the orientation of the osculating plane, and since this is continuously changing, the polarizations of the modes are also changing continuously along the waveguide axis. The net spurious mode amplitude is the sum of the locally generated modes, and to determine this sum it is necessary to resolve the local polarization into two orthogonal polarizations. Furthermore, it has been shown[4] that the same results are obtained by using the curvature of the projections of the waveguide axis on two orthogonal planes. We shall use superscripts $\uparrow$ and $\rightarrow$ to denote the two distinct polarizations, e.g., $TE^{\uparrow}_{pn}$ or $TE^{\rightarrow}_{pn}$. We shall use TE_{pn} with no superscripts in discussions which apply for both polarizations. The two polarizations for the $TM^{\uparrow}_{11}$ and $TM^{\rightarrow}_{11}$ modes are given in Fig. 1. Note that the plane of curvature determines which polarization is generated. The waveguide installed for the field evaluation test has independent curvature characteristics for the two planes, hor-

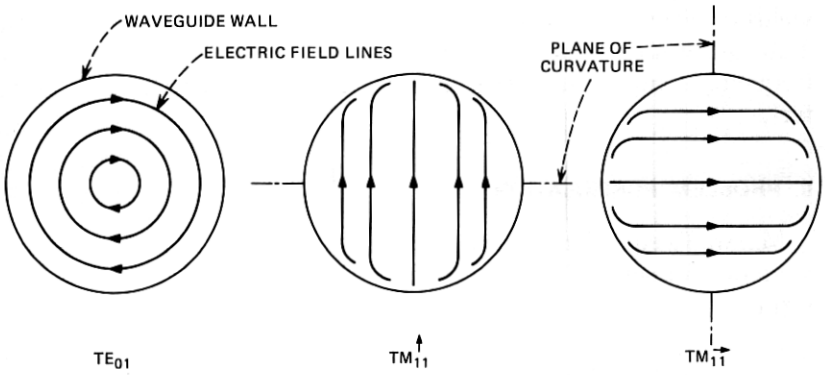

Fig. 1—Normal mode electric fields in dielectric-lined waveguide.

izontal and vertical, shown in Fig. 1, and the polarization of the spurious mode must be carefully accounted for when estimating the TE_{01} loss.

Previous analyses[4] assume $K_{m,n}(z)$ to be sufficiently small so that the total loss can be obtained by a superposition of a number of two mode problems in each of which the TE_{01} mode and one spurious mode is considered. As a specific example, the TE_{01}–TM_{11} mode conversion loss due to axial curvature $c(z)$ in a single plane may be determined from

$$\frac{d}{dz}\begin{bmatrix} A_{01} \\ A_{11} \end{bmatrix} = -j\begin{bmatrix} h_{01} & 0 \\ 0 & h_{11} \end{bmatrix}\begin{bmatrix} A_{01} \\ A_{11} \end{bmatrix} + j\begin{bmatrix} 0 & C_{01,11} \\ C_{01,11} & 0 \end{bmatrix}\begin{bmatrix} A_{01} \\ A_{11} \end{bmatrix} c(z) \quad (2)$$

An approximate[4] expression for the expected TE_{01}–TM_{11} mode conversion loss (α_{01}^{11}) in eq. (2) is

$$\alpha_{01}^{11} = \frac{1}{2} C_{01,11}^2 S_c(\Delta\beta_{01,11}/2\pi) \quad (3)$$

Here S_c is the spectral density function for c and the differential propagation constant $\Delta\beta_{01,11}$ is defined as

$$\Delta\beta_{01,11} = h_{01} - h_{11} \quad (4)$$

Expression (3) is valid in loss-free waveguide, real h_m, and for long lengths of line with a slowly varying power spectrum, S_c.[4] It is an exact solution for (2) in the case of a white power spectrum.[9] Computed power spectral density functions of the installed WT4 field evaluation test waveguide[2,10] diameter, curvature, ellipticity, and higher-order geometric distortions were substituted into the equivalent of (3). The resulting values of loss indicated that approximately 90 percent of the total TE_{01} mode conversion loss, α_{01}^{MC}, was accounted for by $TM_{11}^{\uparrow}$, $TM_{11}^{\rightarrow}$, $TE_{12}^{\uparrow}$, $TE_{12}^{\rightarrow}$ conversions due to the curvatures c_H and c_V of the waveguide axis in the

horizontal and vertical planes, respectively. Thus the predicted mode conversion loss was expected to be

$$\alpha_{01}^{MC} = \frac{1}{2} C_{01,11}^2 \left[S_{cV}(\Delta\beta_{01,11}/2\pi) + S_{cH}(\Delta\beta_{01,11}/2\pi)\right] + \frac{1}{2} C_{01,12}^2 \left[S_{cV}(\Delta\beta_{01,12}/2\pi) + S_{cH}(\Delta\beta_{01,12}/2\pi)\right] \quad (5)$$

The mode conversion loss predicted by (5) differed significantly from the measured loss[10] as discussed in greater detail in Section IV. Moving piston measurements[11] in regions of the field evaluation test line with high curvature indicated the presence of significant levels for the TM_{21} mode as well as TM_{11} and TE_{12} modes.

The measured results implied that second-order conversion processes of the form $TE_{01} \leftrightarrow TM_{11} \leftrightarrow TM_{21}$ are also significant and must be considered along with the first-order processes, $TE_{01} \leftrightarrow TM_{11}$, in estimating the total TE_{01} loss. Instead of considering the two-mode model in (2), we must examine a three-mode model of the form

$$\frac{d}{dz}\begin{bmatrix} A_{01} \\ A_{11} \\ A_{21} \end{bmatrix} = -j \begin{bmatrix} h_{01} & 0 & 0 \\ 0 & h_{11} & 0 \\ 0 & 0 & h_{21} \end{bmatrix} \begin{bmatrix} A_{01} \\ A_{11} \\ A_{21} \end{bmatrix} + j\, c(z) \begin{bmatrix} 0 & C_{01,11} & 0 \\ C_{01,11} & 0 & C_{11,21} \\ 0 & C_{11,21} & 0 \end{bmatrix} \begin{bmatrix} A_{01} \\ A_{11} \\ A_{21} \end{bmatrix} \quad (6)$$

In (6) we are considering only one of the possible TM_{21} conversion paths, as the curvature $c(z)$ is assumed to be in a single plane. The other paths are given in Fig. 2. The coupling model in Fig. 2 leads to the following set of coupled transmission line equations for the determination of TE_{01} mode conversion loss due to curvature of the waveguide axis:

$$\frac{d}{dz}[A] = -j[h][A] + jc_H(z)[C_H][A] + jc_V(z)[C_V][A] \quad (7)$$

where

$$A = [A_{01}, A_{11}^{\uparrow}, A_{12}^{\uparrow}, A_{21}^{\uparrow}, A_{11}^{\rightarrow}, A_{12}^{\rightarrow}, A_{21}^{\rightarrow}]^T \quad (8)$$

Here the A_m's are the transmission line voltages corresponding to the TE_{01}, $TM_{11}^{\uparrow}, \ldots, TM_{21}^{\rightarrow}$ modes. The propagation constants $h_{01}, h_{11}^{\uparrow}, \ldots, h_{21}^{\rightarrow}$ of the modes in straight waveguide are the elements of the diagonal matrix $[h]$. Note that $h_m^{\uparrow} = h_m^{\rightarrow}$ and that no superscript is required for the TE_{01} mode. Corresponding differential propagation constants, $\Delta\beta_{m,n}$ are given in Fig. 3.

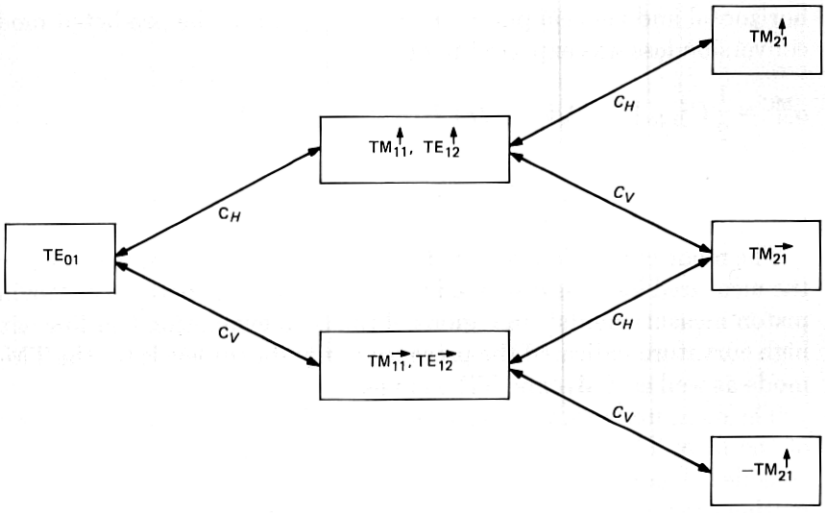

Fig. 2—Curvature coupling mechanisms.

The coupling coefficient matrices $[C_H]$ and $[C_V]$ consist of the normalized curvature coupling coefficients $C_{m,n}$ from mode m to mode n. They may be determined from eq. (57) in the appendix. The normalized curvature coupling coefficients in 60 mm diameter guide, with a 180-μm polyethylene liner are shown in Fig. 4. $[C_H]$ and $[C_V]$ must be multiplied by the local horizontal or vertical curvature, $c_H(z)$ or $c_V(z)$, respectively, to obtain the local coupling coefficients. From Fig. 2 we have

$$j[C_H] = \begin{bmatrix} 0 & jC_{01,11} & jC_{01,12} & 0 & 0 & 0 & 0 \\ jC_{01,11} & 0 & 0 & jC_{11,21} & 0 & 0 & 0 \\ jC_{01,12} & 0 & 0 & jC_{12,21} & 0 & 0 & 0 \\ 0 & jC_{11,21} & jC_{12,21} & 0 & 0 & 0 & 0 \\ 0 & 0 & 0 & 0 & 0 & 0 & jC_{11,21} \\ 0 & 0 & 0 & 0 & 0 & 0 & jC_{12,21} \\ 0 & 0 & 0 & 0 & jC_{11,21} & jC_{12,21} & 0 \end{bmatrix} \quad (9)$$

$$j[C_V] = \begin{bmatrix} 0 & 0 & 0 & 0 & jC_{01,11} & jC_{01,12} & 0 \\ 0 & 0 & 0 & 0 & 0 & 0 & jC_{11,21} \\ 0 & 0 & 0 & 0 & 0 & 0 & jC_{12,21} \\ 0 & 0 & 0 & 0 & -jC_{11,21} & -jC_{12,21} & 0 \\ jC_{01,11} & 0 & 0 & -jC_{11,21} & 0 & 0 & 0 \\ jC_{01,12} & 0 & 0 & -jC_{12,21} & 0 & 0 & 0 \\ 0 & jC_{11,21}jC_{12,21} & & 0 & 0 & 0 & 0 \end{bmatrix} \quad (10)$$

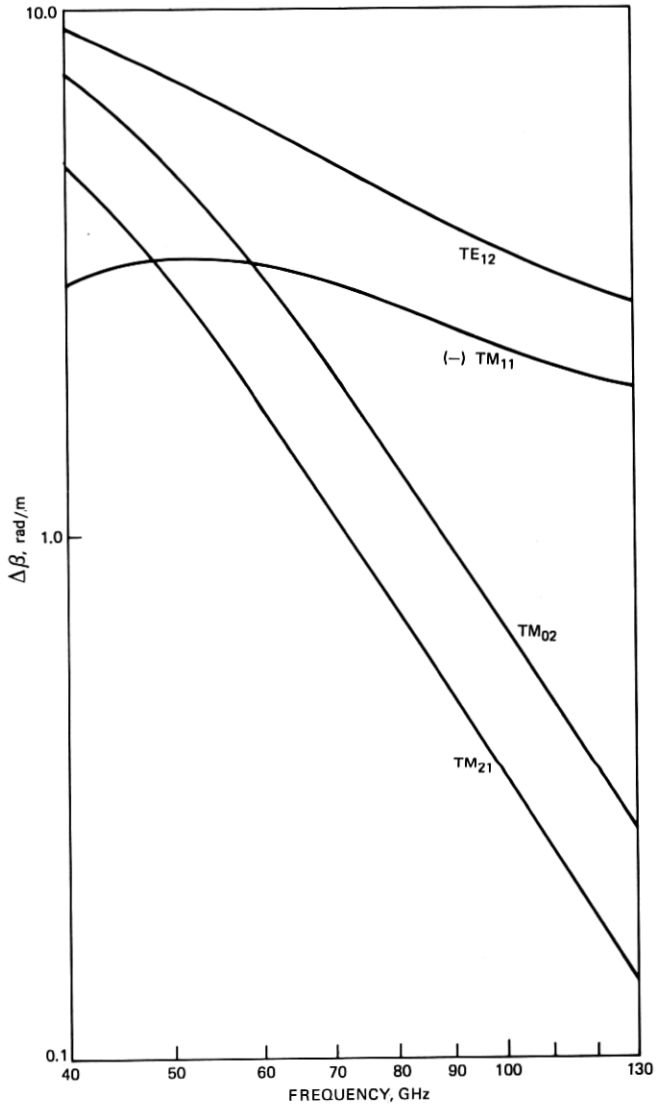

Fig. 3—Differential propagation constants in 60-mm lined waveguide.

Prediction of TE_{01} loss based on the set of coupled line equations in (7) agrees well with measured results as discussed in Section IV.

III. SOLUTIONS—COUPLED LINE EQUATIONS

The set of seven coupled line equations in (7) has been integrated numerically for sets of measured curvature data up to 800 m in length.

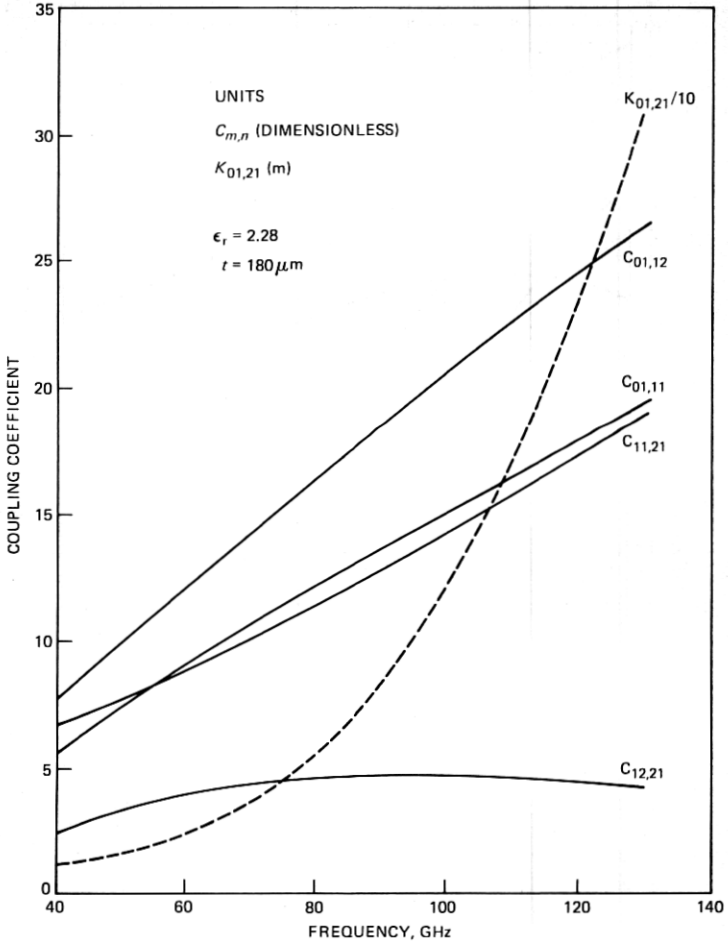

Fig. 4—Coupling coefficients for 60-mm-diameter lined waveguide.

The numerical method yields solutions with an accuracy of better than 1 percent. The method consists of a direct numerical evaluation of the transmission matrix for incremental sections 5 cm long. Direct multiplication of the individual matrices yields the transmission matrix for the desired sections of line. The results agree well with measured data as discussed in Section IV and are a confirmation of the validity of the mode conversion model in Fig. 2. The numerical integration must be carried out at a number of discrete frequencies to determine the loss characteristics over a given frequency band and is an expensive process, since 10 minutes or more of computer time may be required for a 500 m length. Thus approximate solutions are required.

For the case of weak coupling, the seven-mode system of equations in (7) can be reduced to a superposition of three-mode equations similar to (6). It is convenient to define a normalized mode amplitude G_m in terms of A_m

$$A_m = e^{-jh_m z} G_m \tag{11}$$

On applying Picard's method[4] of successive approximations to (6), we find that G_{11} and G_{21} are given to first- and second-order respectively by

$$G_{11} = j \int_0^z C_{01,11} c(s) e^{-j\Delta\beta_{01,11} s} ds \tag{12}$$

$$G_{21} = - \int_0^z C_{11,21} c(s) e^{-j\Delta\beta_{11,21} s} \int_0^s C_{01,11} c(t) e^{-j\Delta\beta_{01,11} t} dt\, ds \tag{13}$$

For slowly varying curvature, $c(z)$, it can be shown that

$$G_{21} \approx j \int_0^z \left\{ C_{11,21} c(s) \left(\frac{C_{01,11}}{\Delta\beta_{01,11}} c(s) \right) \right\} e^{-j\Delta\beta_{01,21} s} ds \tag{14}$$

There is a simple physical interpretation for the terms in (14) which we will examine instead of presenting the details of the analysis. As the TE_{01} mode travels through a region of waveguide with slowly varying curvature in a single plane, the local field structure for the TE_{01} mode is slightly distorted from the structure in the straight waveguide. The degree of distortion can be quantified by expanding the fields in the curved guide in terms of the normal modes for the straight waveguide.[12] In doing so, it is found that the TM_{11} component has a magnitude given by

$$\left(\frac{C_{01,11}}{\Delta\beta_{01,11}} c(z) \right)$$

which is one of the terms in (14). The TM_{11} component travels with the *same* phase velocity as the TE_{01} mode and couples to the TM_{21} mode with a coupling of strength $C_{11,21}\, c(z)$. This is the second coupling term in (14).

Thus the net coupling between the TE_{01} and TM_{21} modes in waveguide with slowly varying curvature, c, is

$$\frac{C_{01,11} C_{11,21}}{\Delta\beta_{01,11}} c^2(z)$$

Equation (14) is similar in form to (12) and thus the three-mode mechanism, $TE_{01} \leftrightarrow TM_{11} \leftrightarrow TM_{21}$, has been converted to an equivalent simple two-mode mechanism $TE_{01} \leftrightarrow TM_{21}$ with an effective normalized

coupling coefficient, $C_{01,21}$, given by

$$C_{01,21} = \frac{C_{01,11}C_{11,21}}{\Delta\beta_{01,11}} \tag{15}$$

The waveguide geometry enters (14) via the factor $c^2(z)$. The reader is cautioned against confusing (15) with the normalized coupling coefficient between the TE_{01} and TM_{21} modes due to ellipticity of the waveguide.

The formula for the expected value of the $TE_{01} \leftrightarrow TM_{21}$ mode conversion loss, α_{01}^{21}, is similar to (3) and is given by

$$\alpha_{01}^{21} = \frac{1}{2} C_{01,21}^2 S_{c^2}(\Delta\beta_{01,21}/2\pi) \tag{16}$$

The loss in (16) is proportional to the spectral density function for the square of the waveguide curvature at a spatial frequency of $\Delta\beta_{01,21}/2\pi$ c/m. From Fig. 3 it may be observed that $\Delta\beta_{01,21}/2\pi$ is less than 0.1 c/m for frequencies greater than 80 GHz, and thus curvatures with long wavelengths, 10m or more are the source of TE_{01}–TM_{21} mode conversion loss in (16).

In Ref. (10) it is shown that the curvature power spectral density for the field evaluation test waveguide in the 0 to 0.1 c/m region of the spectrum is three orders of magnitude larger than the spectrum in the 0.3–1 c/m region which causes TM_{11}, TE_{12} conversion. Thus the assumptions in previous analyses[4] of a slowly varying spectrum are clearly not true and the existence of additional mode conversion loss components is not surprising.

In general, for curvature in two planes, we must consider all of the mechanisms in Fig. 2 to determine the total TE_{01} loss. It is convenient to define an equivalent normalized coupling coefficient, $K_{01,21}$

$$K_{01,21} \equiv 2\left[\frac{C_{01,11}C_{11,21}}{\Delta\bar{\beta}_{11}} + \frac{C_{01,12}C_{12,21}}{\Delta\bar{\beta}_{12}}\right] \tag{17}$$

where

$$\bar{\Delta\beta}_{11} = \frac{\Delta\beta_{11,21} + \Delta\beta_{11,01}}{2}, \quad \bar{\Delta\beta}_{12} = \frac{\Delta\beta_{12,21} + \Delta\beta_{12,01}}{2} \tag{18}$$

A plot of $K_{01,21}$ vs. frequency is given in Fig. 4.

We then find that the mode conversion due to curvature may be approximately treated as a superposition of the two-mode process shown in Table I.

Table I — Mode conversion due to curvature

Conversion process	Geometrical factor	Normalized coupling coefficient	$\Delta\beta$	Loss
TE_{01}–$TM_{11}^{\uparrow}$	c_H	$C_{01,11}$	$\Delta\beta_{01,11}$	$\frac{1}{2}C_{01,11}^2 S_{cH}(\Delta\beta_{01,11}/2\pi)$
TE_{01}–$TM_{11}^{\rightarrow}$	c_V	$C_{01,11}$	$\Delta\beta_{01,11}$	$\frac{1}{2}C_{01,11}^2 S_{cV}(\Delta\beta_{01,11}/2\pi)$
TE_{01}–$TE_{12}^{\uparrow}$	c_H	$C_{01,12}$	$\Delta\beta_{01,12}$	$\frac{1}{2}C_{01,12}^2 S_{cH}(\Delta\beta_{01,12}/2\pi)$
TE_{01}–$TE_{12}^{\rightarrow}$	c_V	$C_{01,12}$	$\Delta\beta_{01,12}$	$\frac{1}{2}C_{01,12}^2 S_{cV}(\Delta\beta_{01,12}/2\pi)$
TE_{01}–$TM_{21}^{\uparrow}$	$c_H^2 - c_V^2$	$K_{01,21}/2$	$\Delta\beta_{01,21}$	$\frac{1}{2}[K_{01,21}/2]^2 S_{c_H^2-c_V^2}(\Delta\beta_{01,21}/2\pi)$
TE_{01}–$TM_{21}^{\rightarrow}$	$c_H c_V$	$K_{01,21}$	$\Delta\beta_{01,21}$	$\frac{1}{2}K_{01,21}^2 S_{c_H c_V}(\Delta\beta_{01,21}/2\pi)$

IV. COMPARISON OF APPROXIMATE AND EXACT SOLUTIONS WITH MEASURED RESULTS

In this section the approximate results obtained in the last section for TE_{01}—TM_{21} mode conversion, the measured results, and the results from a numerical integration of the coupled line equations in (7) are compared for different curvatures of the waveguide axis. Let us first consider an idealized bend, as shown in Fig. 5a, having constant curvature in the horizontal plane and a sinusoidally varying curvature in the vertical plane

$$c_H(z) = 1/R_H$$

$$c_V(z) = A_V \sin \frac{2\pi}{\lambda_m} z \tag{19}$$

From Table I, we can approximately model the $TM_{21}^{\rightarrow}$ conversion process with the following set of two coupled equations. Since $S_{c_H c_V}$ is much greater than S_{cV}^2 and S_{cH}^2 at $\Delta\beta_{01,21}/2\pi$ c/m the $TM_{21}^{\rightarrow}$ level is much greater than the $TM_{21}^{\uparrow}$ level, which is neglected.

$$\frac{d}{dz}A_{01} = -jh_{01}A_{01} + jK_{01,21}\frac{1}{R_H}A_V \sin\left(\frac{2\pi}{\lambda_m}z\right)A_{21}^{\rightarrow}$$

$$\frac{d}{dz}A_{21}^{\rightarrow} = jK_{01,21}\frac{1}{R_H}A_V \sin\left(\frac{2\pi}{\lambda_m}z\right)A_{01} - jh_{21}A_{21}^{\rightarrow} \tag{20}$$

The coupling term in (20), $\sin(2\pi/\lambda_m)z$, is sinuosoidal, and an analytic solution for this case has been obtained by Miller.[13] Miller's solution for (20) will be compared with both the numerical solution and the sec-

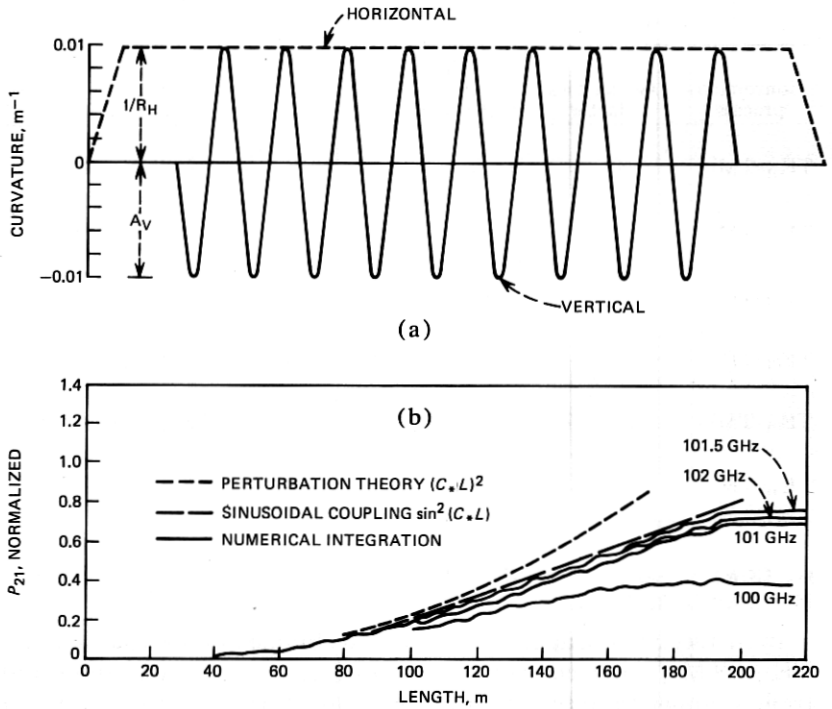

Fig. 5—Comparison of predicted losses for constant curvature bend with sinusoidal curvature in orthogonal plane.

ond-order perturbation theory solution in the following. After the solutions for A_{01} and $A_{21}^{\rightarrow}$ in (20) are determined as in Miller,[13] the normalized $TM_{21}^{\rightarrow}$ level, $G_{21}^{\rightarrow}$, follows from (11):

$$G_{21}^{\rightarrow}(L) = \frac{C_* L \sin\left\{C_* \left|1 + \left(\frac{\Delta\beta_*}{2C_*}\right)^2\right|^{1/2} L\right\}}{\left\{C_* \left|1 + \left(\frac{\Delta\beta_*}{2C_*}\right)^2\right|^{1/2} L\right\}} \tag{21}$$

where

$$C_* = \frac{1}{2} K_{01,21} \frac{1}{R_H} A_V, \qquad \Delta\beta_* = \Delta\beta_{01,21} - \frac{2\pi}{\lambda_m} \tag{22}$$

The corresponding value of G_{01} is

$$|G_{01}(L)|^2 = 1 - |G_{21}^{\rightarrow}(L)|^2 \tag{23}$$

from which the loss is readily obtained. From (14) we obtain the second-order perturbation theory solution for $G_{21}^{\rightarrow}$ for the two curvature

functions in (19) as

$$G_{21}^{\rightarrow}(L) = C_{*}L \tag{24}$$

In Figure 5b, we compare the results from (21) and (24) with a direct numerical integration of the corresponding seven-mode system in (7) for the curvature data in Fig. 5a. We see that there is a substantial disagreement at 100 GHz, the frequency at which $\Delta\beta_{01,21}$ is equal to $2\pi/\lambda_m$, because the propagation constant of TE_{01} in a bend is slightly different from that in the straight waveguide. This causes the frequency at which we obtain coherent coupling to differ slightly from 100 GHz. On performing the numerical integration at a number of frequencies in the vicinity of 100 GHz, it was found that a frequency of 101.5 GHz resulted in a maximum $TM_{21}^{\rightarrow}$ conversion as also shown in Fig. 5b. The 101.5 GHz curve differs by less than 2 percent from the result predicted by (21). The second-order perturbation theory solution in (24) is also in good agreement for small $TM_{21}^{\rightarrow}$ levels, as for $C_{*}L < 0.1$, $C_{*}L \approx \sin C_{*}L$. From the results in Fig. 5 we draw two important conclusions. The equivalent two-mode model in (20) can be summed to give an accurate representation of the seven-mode system in (7) and the second-order perturbation theory solution (14) is valid for small couplings, $C_{*}L < 0.1$.

A controlled experiment was conducted in order to compare the analytic results discussed above with measured data. An experimental bend was constructed having constant curvature in the horizontal plane and either "zero or very small" curvature or a sinusoidally varying curvature in the vertical plane. The measured curvature for this line is given in Fig. 6. Shuttle pulse loss[14] measurements were carried out on this bend for the two different vertical curvature cases. From the difference of the two measurements the loss due to $TM_{21}^{\rightarrow}$ conversion was determined and is shown in Fig. 7 (curve A). Two predicted loss curves are also given in Fig. 7; curve B from a numerical integration of the coupled line equations (7) for the data in Fig. 6, and curve C from the sinusoidal coupling theory (21). There is excellent agreement between all three sets of curves with the exception of some slight frequency shifts. The frequency shift between B and C has been discussed. The shift between A and B is probably due to small errors (<1 percent) in our estimated values for the differential propagation constant $\Delta\beta_{01,21}$.

A similar comparison has been carried out on a 720 m long section in the WT4 field evaluation test. The measured curvature for this section is given in Fig. 8. There are substantial changes in profile in this section and vertical curvatures greater than 0.020 m^{-1} were measured in several regions. The measured loss characteristic for this section is given in Fig. 9. A numerical integration of the coupled line equations, for the measured curvature data in Fig. 8, was carried out at discrete frequencies, as indicated by a circle or cross in Fig. 9 for two cases. The first case allowed

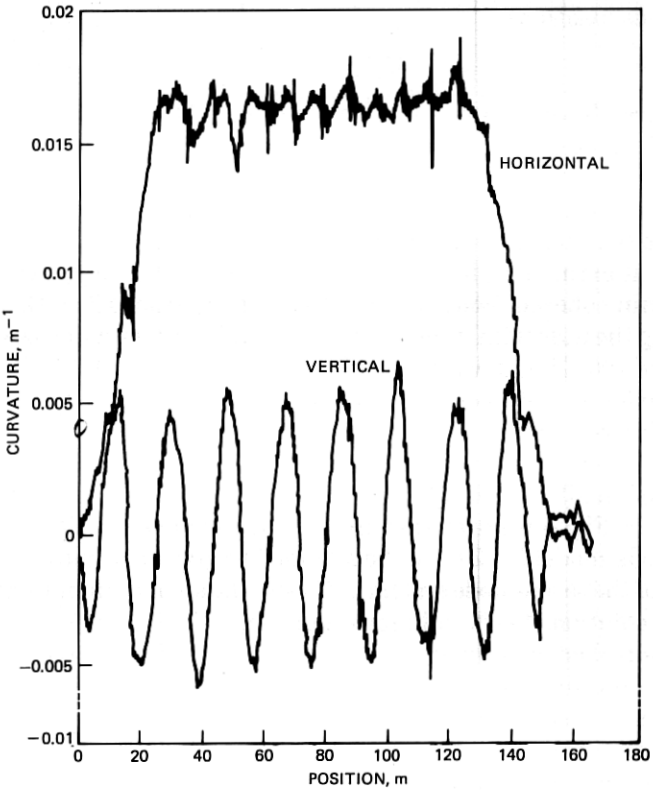

Fig. 6—Measured curvature data for experimental route bend.

only for first order $TM_{11}^{\uparrow}$, $TM_{11}^{\rightarrow}$, $TE_{12}^{\uparrow}$, and $TE_{12}^{\rightarrow}$ conversion, and it can be seen that the predicted losses are much lower than the measured losses. The second case allowed for $TM_{11}^{\uparrow}$, $TM_{11}^{\rightarrow}$, $TE_{12}^{\uparrow}$, $TE_{12}^{\rightarrow}$, $TM_{21}^{\uparrow}$, and $TM_{21}^{\rightarrow}$ conversion. It can be seen in Figure 9 that there is excellent agreement between the measured loss and the numerical integration results. The absolute loss for the peak at 114 GHz is $\approx$ 1.5 dB. This is a fairly large loss, and because of this the perturbation theory will yield losses that are too large. The perturbation theory losses are approximately 30 percent greater than the numerical integration estimate, as also shown in Fig. 9.

The large measured loss peak at 112 GHz is principally due to $TM_{21}^{\uparrow}$ conversion occurring at the large vertical curvature peaks at 125 and 250 m in Fig. 8. This is readily seen in the measured "moving piston" trace of Fig. 10. Here we are measuring[11] the reflected TE_{01} level at the end of the line as a perfectly reflecting piston is moved through this mode filter section in a left-to-right direction in Fig. 8. The large increase in

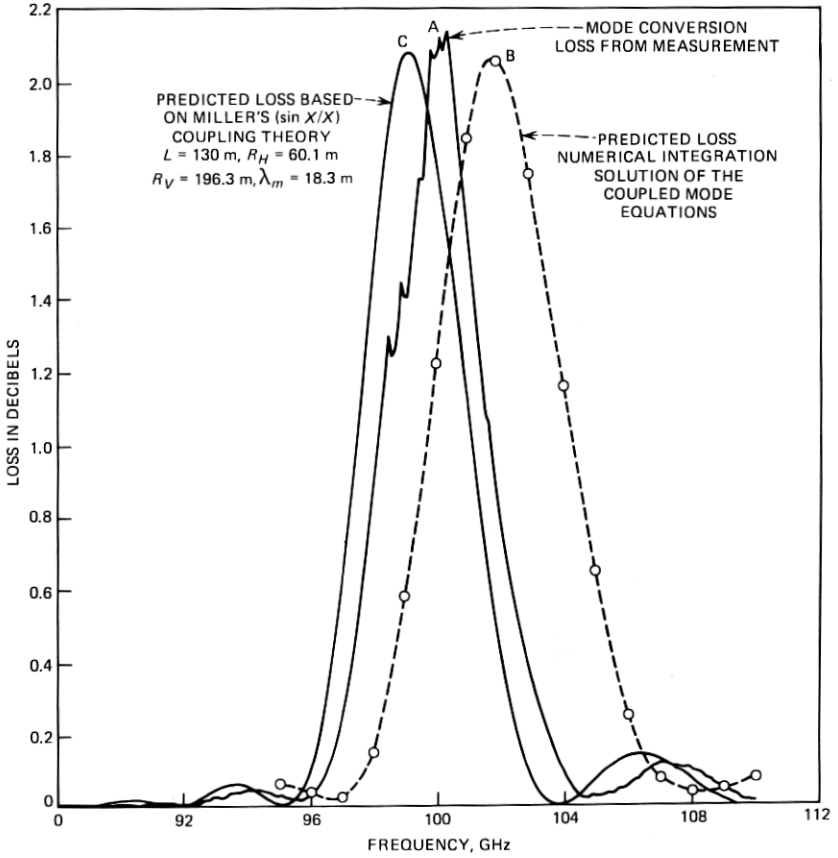

Fig. 7—TE_{01} loss due to mode conversion in modulated bend at Chester.

the TE_{01} ripple at points A and B corresponds to regions of high vertical curvature in Fig. 8.

The numerical integration used in solving (7) consists of an evaluation of the transmission matrix for 5 cm long incremental sections of the waveguide line. A predicted moving piston trace is readily obtained on multiplying the transmission matrix with its transpose. The final result, given in Fig. 11, agrees well with the measured trace in Fig. 10.

V. LOSS VARIATION IN BENDS

In the preceding discussion we have seen that TE_{01}–TM_{21} mode conversion effects result in sizable losses for the TE_{01} mode in bends. This will have a significant impact on repeater siting and spacing for a commercial system and it is desirable to determine the sensitivity of this loss component to system parameters such as guide size (a), frequency

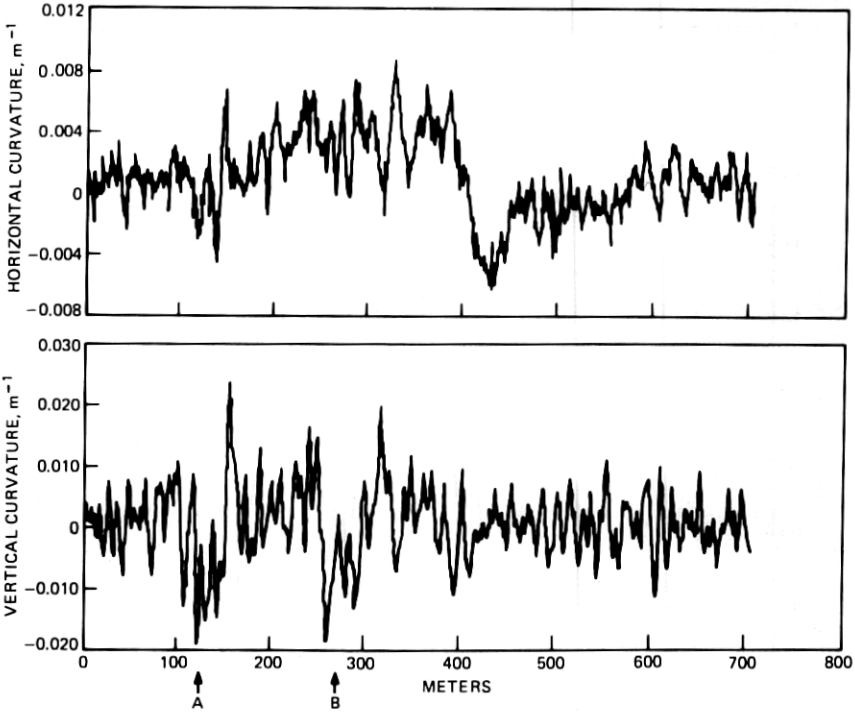

Fig. 8—Measured curvature for 720-m-long section in WT4 field evaluation test.

(f), bend radius (R_B), rms curvature ($c_{V_{\text{rms}}}$), etc. On examination of the loss components in Table I, we see that the TM_{21} loss depends on the product of a coupling coefficient $K_{01,21}$ and a geometrical factor $S_{c_{HcV}}$ or $S_{c_H^2 - c_V^2}$. The coupling coefficient $K_{01,21}$ is the product of two curvature coupling coefficients, e.g., $C_{01,11}$ and $C_{11,21}$ which vary as af, and the inverse of a differential propagation constant, e.g., $\Delta\beta_{01,11}^{-1}$, which varies as $a^2 f$. Thus $K_{01,21}$ varies approximately as $a^4 f^3$. The TM_{21} conversion loss is proportional to $K_{01,21}^2$, and varies as $a^8 f^6$.

In a plan bend with an arc length >100 m and a constant radius R_B < 100 m, the geometrical factor $S_{c_{HcV}}(\Delta\beta_{01,21}/2\pi)$ is approximately equal to $1/{R_B}^2\, S_{c_V}(\Delta\beta_{01,21}/2\pi)$. The magnitude of $S_{c_{HcV}}$ is much greater than in nominally straight waveguide. Thus the TE_{01} loss due to $TM_{21}^{\rightarrow}$ conversion is much greater in a plan bend than in straight waveguide. Conversely, the value of $S_{c_H^2 - c_V^2}(\Delta\beta_{01,21}/2\pi)$ is increased to a lesser degree from the value in straight waveguide for spatial frequencies greater than 0.04 c/m and thus the increase in TE_{01} loss due to $TM_{21}^{\downarrow}$ conversion is of less significance.

With the above assumptions the additional TE_{01} loss per unit length in a plan bend may be approximately written as

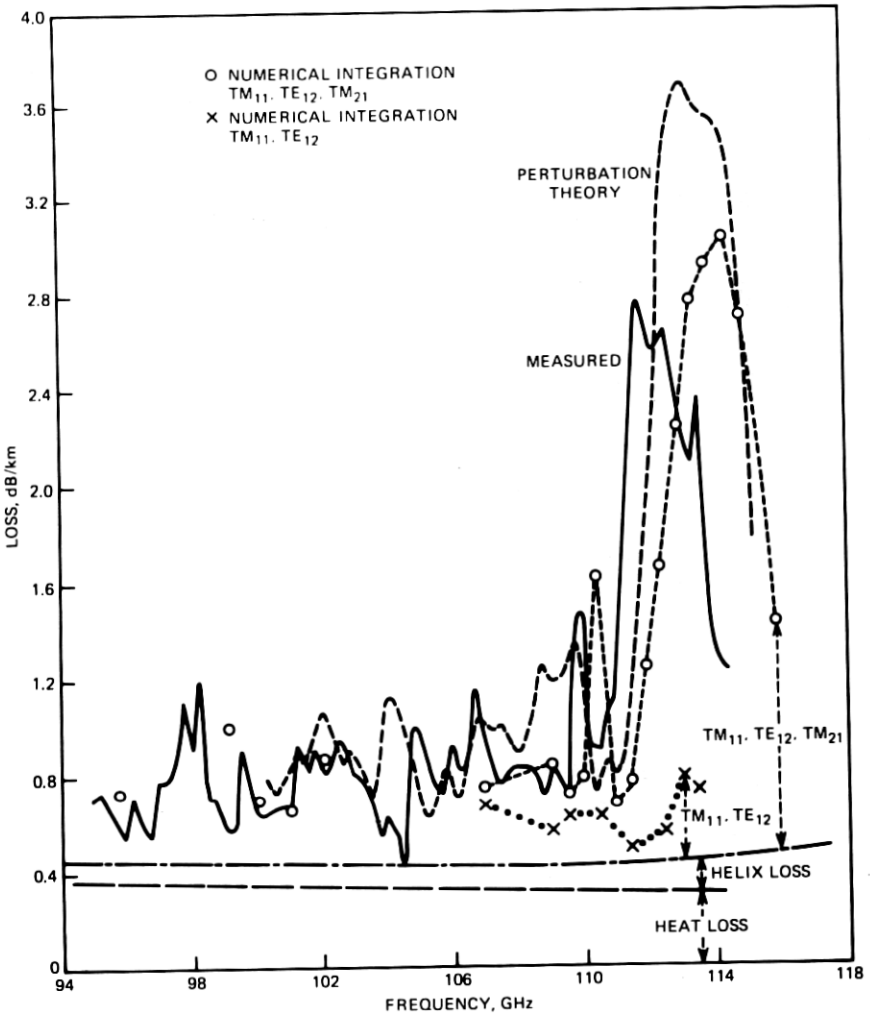

Fig. 9—Loss comparison for 720-m section.

$$\Delta\alpha_{\text{Bend}} = 4.5 \times 10^{-4} \left(\frac{a}{30}\right)^8 \left(\frac{f}{100}\right)^6 \left(\frac{100}{R_B}\right)^2 \left(\frac{S_{cv}}{7 \times 10^{-5}}\right) \quad \text{dB/m} \quad (25)$$

Here a is the guide radius in mm, f is the frequency in GHz, R_B the bend radius in m, and S_{cv} the vertical curvature power spectral density in $1/m^2/c/m$. As an example, from (25) a 95 m radius bend with a net angle of 75 degrees or an arc length of 131 m has an average added loss of 0.12 dB at 110 GHz assuming a value of 7×10^{-5} $1/m^2/c/m$ for S_{cv}. This value of S_{cv} is typical of the WT4 field evaluation test.[10]

Figure 12 is the measured curvature for a bend in the WT4 field evaluation test with nominal parameters similar to those in the preceding

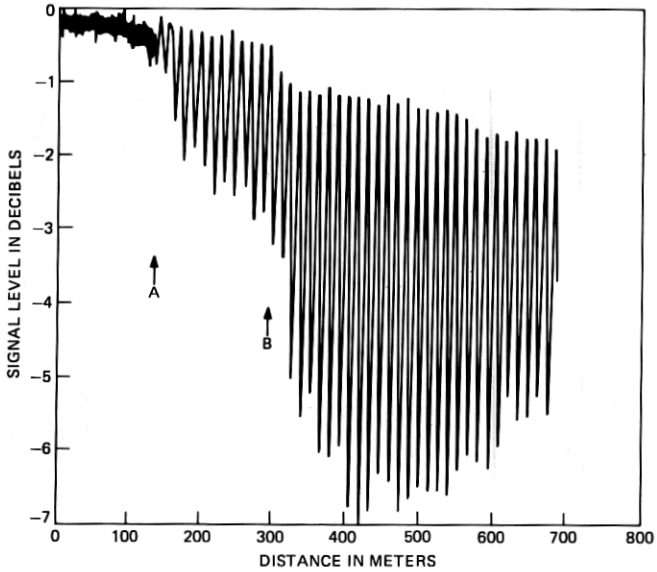

Fig. 10—Moving piston measurement of relative TE_{01} level for 720-m-long section at 113 GHz.

paragraph. The $TM_{21}^{\rightarrow}$ mode conversion loss for this bend was calculated directly using the result of perturbation theory from Table I in Section IV. This agrees fairly well with the numerical integration of the coupled line equation as shown in Fig. 13. Several bends from the field evaluation test were analyzed and exhibited similar agreement. The perturbation theory losses were generally 10 to 20 percent higher than the losses predicted from the numerical integration. The fine structure of the loss, with the exception of small shifts in the loss peaks, was similar for both cases. Figure 13 also gives a comparison of the average added loss predicted from (25) and the actual loss for the bend. In general (25) is useful only for estimating the average loss for a given bend. The actual loss for a given bend exhibits significant fluctuation about this average value as shown in Fig. 13. Any practical installation will contain several route bends in a given repeater span. These bends are independent and thus an expression similar to (25) is useful as it gives an accurate estimate of the average added bend loss.

VI. CONCLUSION

A coupled line system of equations has been presented which predicts the effect of second-order TM_{21} mode conversion on TE_{01} loss. A numerical integration of the coupled line equations developed from this

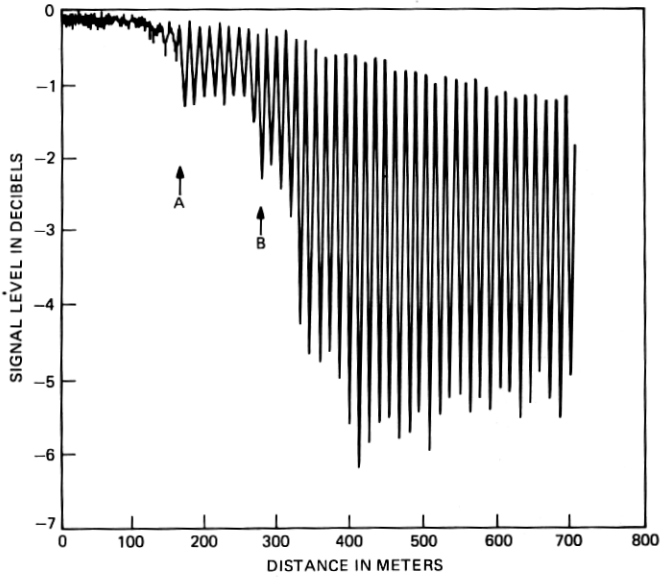

Fig. 11—Calculated TE_{01} level for 720-m-long section at 113 GHz.

model agreed very well with measured results for a bend experiment designed to have high TM_{21} conversion and also agreed with measurements on sections of the WT4 field evaluation test. A second-order perturbation theory solution for the TE_{01} loss due to TM_{21} conversion was derived and discussed. The perturbation theory results agreed well with the results obtained by numerical integration of the coupled line equations for typical sets of curvature data from the WT4 field evaluation test. The perturbation loss estimates were approximately 20 percent higher but the two loss predictions had the same fine structure except for slight shifts in the frequencies of the loss peaks.

An approximate formula for the additional loss due to route bends was given. The added loss is proportional to the inverse square of the bend radius. The added loss increases as the eighth power of guide radius and the sixth power of frequency. The added loss is approximately proportional to the mean squared vertical curvature. This approximate formula works well on the average but does not predict the fine structure of the loss for a given route bend.

There are several areas worthy of further investigation. Additional work is required on the statistics of the TM_{21} mode conversion loss, particularly the loss statistics for a single bend or pair of bends. We have also assumed, without proof, that the TM_{11} and TE_{12} loss is given by the first-order perturbation theory[4] and is little affected by TM_{21} conversion.

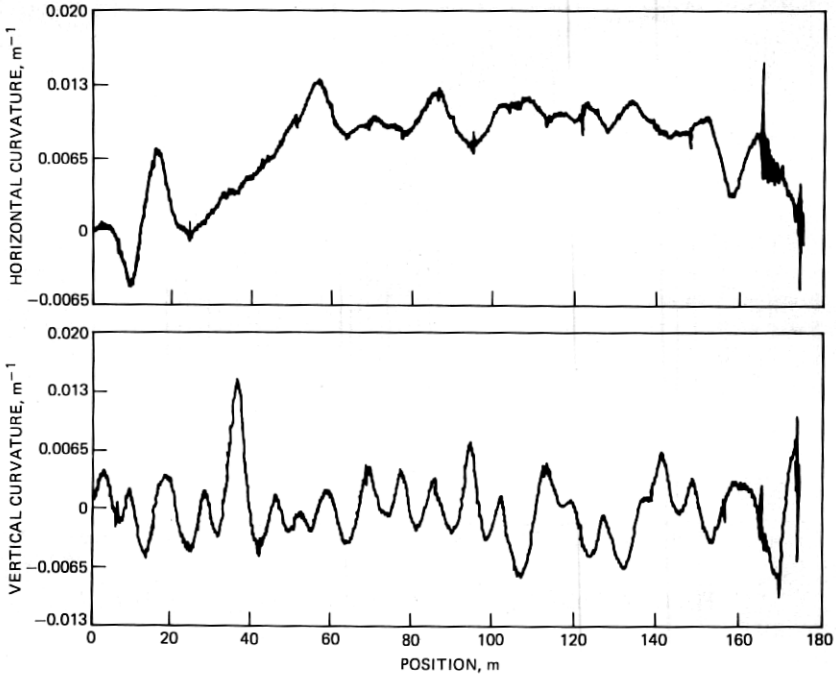

Fig. 12—Measured curvature for plan bend in WT4 field evaluation test.

Note that significant energy passes through these modes to the TM_{21} mode and an examination of higher-order terms is desirable. Finally, the three-mode set of equations (10) has great significance for a practical dielectric-lined waveguide system and is of as much interest as the two-mode systems investigated to date. Improved approximate solutions for systems of this type would be desirable.

ACKNOWLEDGMENT

The authors wish to thank Eli Bochner and Pat Synefakis for their

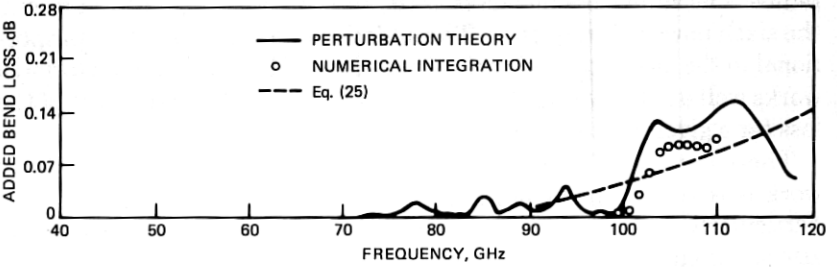

Fig. 13—Added TE_{01} loss for plan bend in WT4 field evaluation test.

assistance with the measurements and computations and Don Rutledge for directing the construction of the experimental route bend.

APPENDIX

Derivation of coupling coefficients

In many cases of interest[1,2,3] circular waveguide with a complex jacket structure may be replaced with a simpler "wall impedance" model with a resultant simplification in the analysis. This is true for the WT4 waveguide and thus we have the following set of equivalent boundary conditions at the inner waveguide surface $r = a$:

$$\begin{aligned} Z_\phi &= E_\phi/H_z|_{r=a} \\ Z_z &= -E_z/H_\phi|_{r=a} \end{aligned} \tag{40}$$

The total fields within the guide can be expressed as a superposition of two scalar functions.

$$\begin{aligned} T_\nu &= N_\nu J_p(x_\nu r) \sin p\phi \\ T'_\nu &= N_\nu J_p(x_\nu r) \cos p\phi \end{aligned} \tag{41}$$

Here ν and p are integers and the eigenvalue $x_\nu a$ is defined by

$$\begin{aligned} k_\nu &= x_\nu a \\ \omega^2\mu_0\epsilon_0 &= k^2 = x_\nu^2 + h_\nu^2 \end{aligned} \tag{42}$$

The fields vary as $e^{-jh_\nu z}$ in the axial direction and k_ν is the solution of the characteristic equation

$$j\omega\epsilon_0 a Z_z$$

$$- \frac{k_\nu J_p(k_\nu)\left[J'_p(k_\nu) + j\omega\epsilon_0 Z_\phi \frac{x_\nu}{k^2} J_p(k_\nu)\right]}{-\frac{p}{k_\nu^2}\frac{h_\nu^2}{k^2} J_p^2(k_\nu) + J'_p(k_\nu)\left[J'_p(k_\nu) + j\omega\epsilon_0 Z_\phi \frac{x_\nu}{k^2} J_p(k_\nu)\right]} = 0 \tag{43}$$

The total fields are expressible as a superposition of normal mode fields

$$\overline{E} = \sum_\nu A_\nu^+(z)\overline{e}_\nu^+ e^{-jh_\nu z} + \sum_\nu A_\nu^-(z)\overline{e}_\nu^- e^{+jh_\nu z} \tag{44}$$

$$\overline{H} = \sum_\nu A_\nu^+(z)\overline{h}_\nu^+ e^{-jh_\nu z} + \sum_\nu A_\nu^-(z)\overline{h}_\nu^- e^{+jh_\nu z}$$

where

$$\begin{aligned} \overline{e}_\nu^\pm = \hat{r}\sqrt{\frac{h_\nu}{\omega\epsilon_0}}\left(\frac{\partial T_\nu}{\partial r} + d_\nu \frac{\partial T'_\nu}{r\partial\phi}\right) + \hat{\phi}\sqrt{\frac{h_\nu}{\omega\epsilon_0}}\left(\frac{\partial T_\nu}{r\partial\phi} - d_\nu \frac{\partial T'_\nu}{\partial r}\right) \\ + \hat{z}(\pm)j\omega\mu_0\sqrt{\frac{\omega\epsilon_0}{h_\nu}}\frac{x_\nu^2}{k^2} T_\nu \end{aligned} \tag{45}$$

$$\bar{h}_\nu^{\pm} = \hat{r}(\mp)\sqrt{\frac{\omega\epsilon_0}{h_\nu}}\left(\frac{\partial T_\nu}{r\partial\phi} - d_\nu\frac{h_\nu^2}{k^2}\frac{\partial T_\nu'}{\partial_r}\right)$$
$$+ \hat{\phi}(\pm)\sqrt{\frac{\omega\epsilon_0}{h_\nu}}\left(\frac{\partial T_\nu}{\partial r} + d_\nu\frac{h_\nu^2}{k^2 r\partial\phi}\frac{\partial T_\nu'}{}\right) + \hat{z}j\omega\epsilon_0\sqrt{\frac{h_\nu}{\mu\epsilon_0}}\,d_\nu\frac{x_\nu^2}{k^2}T_\nu'$$

The separation constant d_ν is given by

$$d_\nu = \frac{p}{k_\nu^2}\left\{y_\nu + \frac{j\omega\epsilon_0 a Z_\phi}{k^2a^2}\right\}^{-1}$$
$$= \frac{k_\nu^2}{p}\frac{k^2}{h_\nu^2}(y_\nu + j/\omega\epsilon_0 a Z_z) \tag{46}$$
$$y_\nu = J_p'(k_\nu)/k_\nu J_p(k_\nu)$$

The modes are orthonormal as the vector cross product

$$\int\int_s \bar{e}_\mu^{+}\mathrm{x}\bar{h}_\nu^{\pm}\cdot d\bar{s} = \pm\,\delta_{\nu\mu} \tag{47}$$

The normalization constant N_ν is given by

$$\frac{\pi}{2}N_\nu^2k_\nu^2J_p^2(k_\nu)\left[\left(1+\frac{d_\nu^2h_\nu^2}{k^2}\right)\left(1-\frac{p^2}{k_\nu^2}+2y_\nu+k_\nu^2y_\nu^2\right)\right.$$
$$\left. - 2\left(1+\frac{h_\nu^2}{k^2}\right)d_\nu\frac{p}{k_\nu^2}\right] = 1 \tag{48}$$

for $p \neq 0$, and by

$$\pi N_\nu^2k_\nu^2J_0^2(k_\nu)\frac{d_\nu^2h_\nu^2}{k^2}\{(1+k_\nu^2y_\nu^2+2y_\nu)\} = 1 \tag{49}$$

for $TE_{0\nu}$ modes, and by

$$\pi N_\nu^2k_\nu^2J_0^2(k_\nu)\{(1+k_\nu^2y_\nu^2+2y_\nu)\} = 1 \tag{50}$$

for $TM_{0\nu}$ modes.

For a nonideal waveguide where the inner surface is of the form $r = a + \epsilon\rho_1(\phi,z)$ where $\epsilon \ll 1$, we may express the total field in the distorted guide $(\bar{E},\bar{H})$ as a superposition of the normal modes[5] in an ideal guide of radius a. On taking Maxwell's equations, multiplying by $\bar{h}_\mu^{\pm}$ or $\bar{e}_\mu^{\pm}$, integrating by parts over the guide cross section and adding we find

$$\int\int_s (\nabla\times\bar{E} = -j\omega\mu_0\bar{H})\cdot\bar{h}_\mu^{\pm}\,ds + \int\int_s (\nabla\times\bar{H} = j\omega\epsilon_0\bar{E})\cdot\bar{e}_\mu^{\pm}\,ds$$

reduces to

$$\frac{\partial}{\partial z}A_\mu^{\pm}(z) = \pm\frac{1}{2}\left\{\oint_{r=a}\bar{E}\times\bar{h}_\mu^{\pm}\cdot\hat{r}\,dl + \oint_{r=a}\bar{H}\times\bar{e}_\mu^{\pm}\cdot\hat{r}\,dl\right\} \tag{51}$$

We now apply the boundary condition in (1) at $r = a + \epsilon\rho_1(\phi,z)$. For any initial field $\overline{E}_0$, $\overline{H}_0$ in undistorted guide the distortion $\epsilon\rho_1$ yields a distorted field $\overline{E}$, $\overline{H}$ to first order of

$$\begin{aligned} \overline{E} &= \overline{E}_0 + \epsilon\overline{E}_1 \\ \overline{H} &= \overline{H}_0 + \epsilon\overline{H}_1 \end{aligned} \tag{52}$$

At $r = a + \epsilon\rho_1$ we have to first order from (40)

$$\frac{1}{a}\frac{\partial\rho_1}{\partial\phi}E_{0r} + \rho_1\frac{\partial E_{0\phi}}{\partial r} + E_{1\phi} = Z_\phi\left\{\frac{\partial\rho_1}{\partial z}H_{0r} + \rho_1\frac{\partial H_{0z}}{\partial r} + H_{1z}\right\} \tag{53}$$

$$\frac{\partial\rho_1}{\partial z}E_{0r} + \rho_1\frac{\partial E_{0z}}{\partial r} + E_{1z} = -Z_z\left\{\frac{1}{a}\frac{\partial\rho_1}{\partial\phi}H_{0r} + \rho_1\frac{\partial H_{0\phi}}{\partial r} + H_{1\phi}\right\}$$

From (51) we need to determine

$$[\overline{E}\times\overline{h}_\mu^{\mp} + \overline{H}\times\overline{e}_\mu^{\mp}]|_{r=a}\cdot\hat{r}$$

On substituting [from (52)] for $\overline{E}$ and $\overline{H}$ and using boundary conditions (40) at $r = a$ for $\overline{E}_0$ and $\overline{H}_0$ we find

$$[\overline{E}\times\overline{h}_\mu^{\mp} + \overline{H}\times\overline{e}_\mu^{\mp}]\cdot\hat{r}|_a = \epsilon[\overline{E}_1\times\overline{h}_\mu^{\mp} + \overline{H}_1\times\overline{e}_\mu^{\mp}]\cdot\hat{r}|_a \tag{54}$$

The right-hand side of (54) may be reduced to terms containing only $\overline{E}_0$, $\overline{H}_0$, and $\overline{h}_\mu^{\mp}$ by expanding and substituting for $(E_{1\phi} - Z_\phi H_{1z})$ and $(E_{1z} + Z_z H_{1\phi})$ from (53).

On letting

$$\overline{E}_0 = \sum_\nu A_\nu\overline{e}_\nu \quad\text{and}\quad \overline{H}_0 = \sum_\nu A_\nu h_\nu^-$$

we finally obtain a system of coupled equations of the form

$$\frac{\partial}{\partial z}A_\mu^+(z) = \sum_\nu K_{\mu\nu}^{(+,+)}A_\nu^+(z)e^{j(h_\mu - h_\nu)z} + K_{\mu\nu}^{(+,-)}A_\nu^-(z)e^{j(h_\mu+h_\nu)z} \tag{55}$$

Only forward coupling is significant as $h_\nu \approx h_\mu$ and we need concern ourselves only with the forward coupling coefficient, $K_{\mu,\nu}^{(+,+)}$ which is of the form

$$K_{\mu,\nu}^{(+,+)} = \frac{1}{2}\int_0^{2\pi}\epsilon\left\{-h_{\mu\phi}\left[\frac{\partial\rho_1}{\partial_z}e_{\nu r} + \rho_1\frac{\partial e_{\nu z}}{\partial r} + Z_z\left(\frac{1}{a}\frac{\partial\rho_1}{\partial\phi}h_{\nu r} + \rho_1\frac{\partial h_{\nu\phi}}{\partial r}\right)\right]\right.$$

$$\left. + h_{\mu z}\left[-\frac{1}{a}\frac{\partial\rho_1}{\partial\phi}e_{\nu r} - \rho_1\frac{\partial e_{\nu\phi}}{\partial r} + Z_\phi\left(\frac{\partial\rho_1}{\partial z}h_{\nu r} + \rho_1\frac{\partial h_{\nu z}}{\partial r}\right)\right]\right\}a\,d\phi \tag{56}$$

This is similar to Unger's[15] result for helix waveguide ($Z_\phi = 0$) coupling coefficients but contains several additional terms.

$K_{\mu,\nu}^{+,+}$ is the coupling coefficient for displacement of the waveguide walls from a right circular cylinder. If $\rho_1(\phi,z)$ is of the form

$$\epsilon\rho_1(\phi,z) = \epsilon \cos \phi f(z)$$

we can determine the curvature coupling coefficient ($C^{+,+}_{\mu,\nu}$) from $K^{+,+}_{\mu,\nu}$ as in Rowe and Warters. Since the curvature $1/R(z)$ is approximately equal to $-\epsilon f''(z)$ we have

$$C^{(+,+)}_{\mu,\nu} = K^{(+,+)}_{\mu,\nu}/[j(h_\mu - h_\nu)]^2 \tag{57}$$

This is the normalized curvature coupling coefficient referred to in the main text of this paper.

REFERENCES

1. D. A. Alsberg et al., "WT4 Millimeter-Wave Transmission System Overview," B.S.T.J., this issue.
2. R. D. Tuminaro et al., "Waveguide Design and Fabrication," B.S.T.J., this issue.
3. S. A. Schelkunoff, "Conversion of Maxwell's Equations into Generalized Telegraphists Equations," B.S.T.J., *34,* No. 7 (September 1955), pp. 995–1043.
4. H. E. Rowe and W. D. Warters, "Transmission in Multimode Waveguide with Random Imperfections," B.S.T.J., *41,* No. 5 (May 1962), pp. 1031–1170.
5. S. P. Morgan, "Mode Conversion Losses in Transmission of Circular Electric Waves through Slightly Noncylindrical Guides," J. Appl. Phys., *21,* April 1950, pp. 329–338.
6. H. G. Unger, "Lined Waveguide," B.S.T.J., *41,* No. 3 (March 1962), pp. 745–768.
7. H. L. Kreipe and H. G. Unger, "Imperfections in Lined Waveguide," B.S.T.J., *41,* No. 7 (September 1962), pp. 1589–1619.
8. J. W. Carlin and P. D'Agostino, "Normal Modes in Overmoded Dielectric Lined Circular Waveguide," B.S.T.J., *52,* No. 4 (April 1973), pp. 453–486.
9. H. E. Rowe and D. T. Young, "Transmission Distortion in Multimode Random Waveguides," IEEE Trans. Microwave Theory Tech., *MTT-20,* June 1972, pp. 349–365.
10. J. C. Anderson et al., "Field Evaluation Trial—Medium Objectives and Results," B.S.T.J., this issue.
11. M. A. Gerdine et al., "Electrical Transmission Measurement System," B.S.T.J., this issue.
12. H. G. Unger, "Circular Electric Wave Transmission in Dielectric-Coated Waveguide," B.S.T.J., *36,* No. 7 (September 1957), pp. 1253–1278.
13. S. E. Miller, "Some Theory and Application of Periodically Coupled Waves," B.S.T.J., *48,* No. 7 (September 1969), pp. 2189–2219.
14. A. P. King and G. D. Mandeville, "The Observed 33–90 kMc Attenuation of 2-Inch Improved Waveguide," B.S.T.J., *40,* No. 7 (September 1961), pp. 1323–1330.
15. H. G. Unger, "Noncylindrical Helix Waveguide," B.S.T.J., *40,* No. 1 (January 1961), pp. 233–254.